Linear Homeomorphic Model for Human Movement

A. TERRY BAHILL, MEMBER, IEEE, JOSE R. LATIMER, AND B. TODD TROOST

Abstract—**The parameter values for this model are specific to the human eye movement systems; however, the form of the model is applicable to other neurological motor control systems. The muscle length-tension diagram was modeled with an ideal spring. The muscle force-velocity relationship was linearized in a manner that produced a linear model. Initial parameter estimates were based on physiological data, human when possible. Then a function minimization program was used to fine tune model parameters. These parameter values were compared to the original physiological data to ensure that they were within the range of variability of the data. The antagonist dashpot value was selected to minimize the mean squared error between human and model responses; the value produced suggested a unique simplified representation for the original physiological data. The parameter estimation routine was applied to make the model match atypical human eye movements; these simulations suggested that glissades in normals are caused by pulsewidth, not pulse height errors.**

I. INTRODUCTION

THE OCULAR motor system is ideal for studying the control of human movement: eye movements are easy to measure, and the control of saccadic eye movements is simpler than the control of other neuromuscular systems. It is simpler because the load presented by the eyeball and extraocular tissues is small and constant. Horizontal eye movements offer a further simplification because they primarily involve only two muscles of each eye. By scrutinizing the trajectories of saccadic eye movements, we can infer the motoneuronal activity, deduce the central nervous system's control strategy, and observe changes in this control strategy caused by fatigue, alcohol, drugs, or pathology. These eye movement control principles should generalize to other neuromuscular systems.

An initial step in understanding this movement control system is the development of an appropriate descriptive model. One of the first eye movement models was developed by Descartes [1] in 1630 to illustrate his discovery of the principle of reciprocal innervation. The next model was a linear second-order model proposed by Westheimer [2] in 1954. The input to the model was assumed to be a step of muscle force. This model worked well for 10° saccades, but not for saccades of any other size. In 1964 Robinson [3] showed that the actual input signal looked more like a pulse-step of muscle force. His linear fourth-order model could simulate saccades between 5° and 40°. However, in 1968 it was pointed out [4] that the velocity profiles generated by his model were not realistic. Cook and Stark's sixth-order nonlinear model [4] did produce realistic velocity profiles. Parameter values and the treatment of the nonlinear force-velocity relationship were changed in subsequent versions [5]-[7] to yield the reciprocal innervation model, which produced realistic position, velocity, and acceleration records for saccadic eye movements ranging from 0.1° to 50°. It also simulated smooth pursuit and vergence eye movements, given appropriate input signals. A sensitivity analysis of the model parameters was performed [7], and the model was validated qualitatively, quantitatively, analytically, and heuristically [8]. This model formed the starting point for the studies presented here.

In these previous models, length-tension diagrams from cat experiments were used. The maximum isometric force for the feline's medial and lateral rectus muscles occurs when the muscle length is near the primary position (looking straight ahead) rest-length. For small variations around this length the force would be constant. This approximation made it appear that the length-tension characteristics were not incorporated into the model. However, data from human experiments [9]-[11] show that this rest-length relation is not valid for the human horizontal recti, where the length at primary position is shorter than the length for maximum isometric force. These human data were used to formulate the length-tension element in our current model.

The relationship between force and velocity is an important characteristic of contracting muscles. The force-velocity curves for a shortening muscle are roughly hyperbolic [12]. Numerical values for the force and velocity axes intercepts are unique for each muscle. The velocity axis intercept v_{max} is the maximum isotonic contraction velocity for the muscle under study. The previous models derived this constant from cat experiments. They used 3600°/s for the velocity axis intercept v_{max}. This value is four times larger than the maximum recorded human extraocular eye muscle velocity and is more than twice as large as the maximum velocity of θ_2 in the model. The sensitivity analysis [7] showed that this parameter was the fourth most important parameter in the model. For these reasons this parameter was reformulated in our present model.

Manuscript received October 4, 1979; revised July 1, 1980. This work was supported by the National Science Foundation under Grant ENG 7722418.

A. T. Bahill is with the Biomedical Engineering Program and the Department of Electrical Engineering, Carnegie-Mellon University, Pittsburgh, PA 15213, and the Department of Neurology, University of Pittsburgh Medical School, Pittsburgh, PA 15261.

J. R. Latimer was with the Biomedical Engineering Program and the Department of Electrical Engineering, Carnegie-Mellon University, Pittsburgh, PA 15213. He is now with the Strategic Systems Department, Applied Physics Laboratory, The Johns Hopkins University, Baltimore, MD 21218.

B. T. Troost was with the Biomedical Engineering Program, Carnegie-Mellon University, Pittsburgh, PA 15213, the Department of Neurology, University of Pittsburgh, Pittsburgh, PA 15261, and the Veterans Administration Medical Center, Pittsburgh, PA 15240. He is now with the Department of Neurology, Case Western Reserve University, Cleveland, OH 44106, and the Neurology Service, Veterans Administration Medical Center, Cleveland, OH 44106.

0018-9294/80/1100-0631$00.75

Nonlinearities of the model are due to this nonlinear force-velocity relationship which is modeled as a nonlinear dashpot. Clark and Kamat (in [13] tried to linearize the model by using a Taylor series expansion on the model (excluding second and higher order terms). The linear perturbation equations were not trivial to solve and the implementation of a known nominal solution was cumbersome. The oversimplification of neglecting the activation and deactivation time constants was the most likely reason that their linear model did not match physiological data. In another effort to linearize the model, Latimer *et al.* [14] plotted numerical values for the dashpots representing the apparent viscosities of the muscles. Straight line approximations of these time functions closely fit the actual values of the dashpots for a 10° saccade. The nonlinear problem was thereby transformed into a time variant problem, which was still cumbersome.

The most obvious method of linearizing is to approximate the force-velocity curves with straight lines. Stark [15], in formulating the BIOSIM simulation language, approximated these curves with straight lines through the point of maximum velocity (v_{max}). This linearized the force-velocity relationship, but did not linearize the model because the dashpot parameters became functions of the model states [14]. The incorporation of additional physiological data allows a linearization of the force-velocity relationship resulting in the linear homeomorphic model which is presented here.

II. Results

A. Length-Tension Diagram

The maximum contractile force a muscle can generate depends, in part, on its length. Muscle forces generated when the muscle is contracted are weaker than the maximum forces. A curve of the length-tension contribution to the dynamic contractile force of a muscle and the purely passive contribution due to the muscle's inherent elastic resistance to stretch appear in Fig. 1.

The linearity, constant slope, and parallel lines can be explained by the sliding filament model for muscle [16]. Force developed is linearly proportional to the shortening or lengthening from the primary rest-length. Over the range of normal eye movements the horizontal recti operate within this linear range of force and length.

The length-tension diagram can be simulated with the model of Fig. 2. The force generator F is called the *active state tension generator*. The distance L' is a hypothetical reference length and L is the muscle length. T is the tension in the muscle, which is also the force exerted on the eye by the muscle. The static equations for equilibrium are

$$T = F + K_{LT}L' \tag{1}$$

$$T = K_{SE}(L - L'). \tag{2}$$

We can solve for L' in (2), substitute this into (1), and rearrange to get

$$T = \frac{K_{LT}K_{SE}L}{K_{LT} + K_{SE}} + \frac{K_{SE}F}{K_{LT} + K_{SE}}. \tag{3}$$

The above equation for length-tension will produce the curves

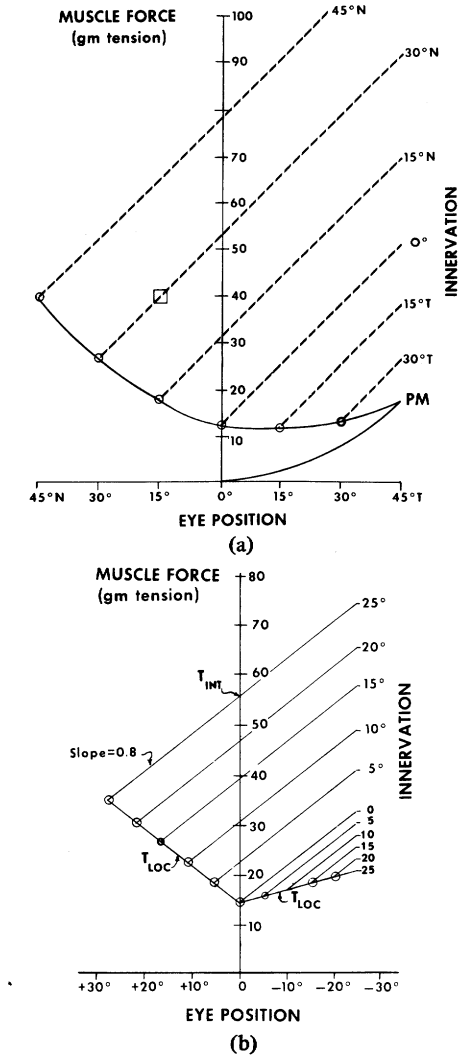

Fig. 1. (a) Human and (b) linear model length-tension diagrams. The human data were recorded during strabismus surgery. One horizontal rectus muscle was detached from the eyeball and connected to a force transducer. Then the subject was instructed to look at a target with his unoperated eye. For example, when the subject was asked to look at a target 30° nasal (N) of primary position with his good left eye, and the medial rectus muscle of the operated right eye was held in a position appropriate for 15° nasal of primary position, a 40 gm force was recorded (the box). The circles indicate muscle forces for a normal fixating eye. *PM* is the curve for passive muscle. Temporal gaze is represented by the symbol T. Human physiological data [9], [10] were averaged together to produce (a). The curves of (b) fell within the range of variability of the human data.

of Fig. 1(b), which model the simplified human data of Fig. 1(a). The slope of these curves K' is given in the length-tension equation (3) as

$$K' = \frac{K_{LT}K_{SE}}{K_{LT} + K_{SE}}.$$

Since K_{SE} is approximately 125 N/m (2.5 gm tension/°) [11], and K' can be read from the graph of Fig. 1(a) as 40 N/m (0.8 gm tension/°), K_{LT} can be calculated.

$$K_{LT} = \frac{K_{SE}K'}{K_{SE} - K'}$$

$$K_{LT} = 60 \text{ n/m} = 1.2 \text{ gm tension/°}. \tag{4}$$

The intersections of the dashed lines and the parabolic curve

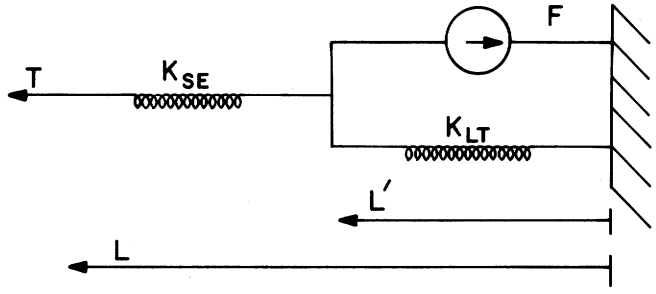

Fig. 2. Simplified mechanical model for human muscle. The active state tension generator is modeled with the ideal force generator F; the series elasticity and the length-tension diagram are modeled with ideal springs, K_{SE} and K_{LT}.

in Fig. 1(a), the circles, represent the fixation forces for the stationary eye, that is, the tension T required to hold the eye at various angles of gaze. A two piece linear approximation to this solid parabolic curve is shown in Fig. 1(b). This straight line approximation is incorporated into the extraocular plant model. The agonist fixation forces T_{LOC} are given by

$$T_{LOC} = 14 + 0.8\theta$$

where θ is the commanded final eye position. The muscle tension axis ($\theta = 0$) intercept T_{INT} is found by

$$T_{INT} = T_{LOC} + K'\theta = T_{LOC} + 0.8\theta = 14 + 1.6\theta \quad (5)$$

Another equation for T_{INT} can be obtained by setting $L = 0$ in (3) to yield

$$T_{INT} = \frac{K_{SE}F}{K_{LT} + K_{SE}}.$$

The force F is that produced by the active state tension generator. For the steady-state behavior of the agonist muscle, this steady-state force is defined to be the neural activity $N_{AG\text{-}STEP}$. Now, (5) and (6) can be combined to yield

$$14 + 1.6\theta = \frac{K_{SE}}{K_{LT} + K_{SE}} N_{AG\text{-}STEP}$$

$$N_{AG\text{-}STEP} = \frac{(14 + 1.6\theta)(K_{LT} + K_{SE})}{K_{SE}}$$

$$N_{AG\text{-}STEP} = (20.6 + 2.35\theta) \text{ gm tension.} \quad (7)$$

The same steps can be performed for the antagonist.

$$T_{LOC} = 14 + 0.3\theta$$

$$T_{INT} = T_{LOC} - 0.8\theta = 14 - 0.5\theta$$

$$14 - 0.5\theta = \frac{K_{SE}}{K_{LT} + K_{SE}} N_{ANT\text{-}STEP}$$

$$N_{ANT\text{-}STEP} = (20.6 - 0.74\theta) \text{ gm tension.} \quad (8)$$

B. Force-Velocity Relationship Linearization

Previous models have been nonlinear because the force-velocity data were fit with a family of hyperbolas through a fixed point on the velocity axis (v_{max}). However, physiological data has shown that v_{max} varies with the motoneuronal activity [17]-[21]. Thus, a better linearization would be a family of piecewise linear curves with equal, constant slopes, shown with straight lines in Fig. 3.

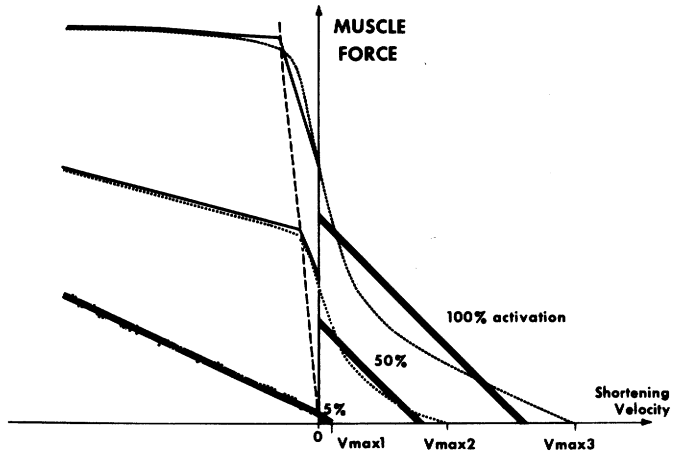

Fig. 3. Force-velocity relationship for muscle (dotted lines) and the linear model (solid lines). For normal movements the agonist muscle will use the upper curves in the first quadrant and the antagonist muscle will use the lower curve in the second quadrant (the thickened lines). The parameter estimation routine showed that for low values of innervation the antagonist curve is best fit with only one straight line. This greatly simplifies the model.

When a muscle is stimulated and quickly stretched, it offers a high resistance to the external force. This antagonist force-velocity relationship can be modeled by a two piece linear approximation as shown in Fig. 3. The intersection of these two lines is a linear force dependent function. During normal saccadic movements the antagonist muscle force is reduced, corresponding to less than 2 percent of maximum innervation. Our parameter estimation algorithm [22] was used in an attempt to find the intersection and slopes of the piecewise approximations of the force-velocity curves using a 10° saccade. The results showed that the best fit to the data was obtained by using only one line for the force-velocity approximation of the 2 percent innervation curve [22]. This unexpected result greatly simplified the linearization of the force-velocity relationship.

The parameter estimation routine produced the following constant slopes for the force-velocity relstionship:

$$B_{AG} = 2.36 \text{ N} \cdot \text{s/m} = 0.046 \text{ gm tension} \cdot \text{s/}^\circ \quad (9)$$

$$B_{ANT} = 1.12 \text{ N} \cdot \text{s/m} = 0.022 \text{ gm tension} \cdot \text{s/}^\circ. \quad (10)$$

The force-velocity relationship shows that muscles produce larger forces at lower velocities. It is as if there was an internal dashpot decrementing the force available from the active state tension generator. This is just how the force-velocity relationship is modeled in Fig. 4: the muscle force available at the tendon is decreased by a velocity dependent term, an apparent viscosity.

In the previous section we derived an equation (3) representing the force available at the tendon after the active state tension was modified by the effects of the length-tension diagram. We can change into variables appropriate for rotations by letting $\theta_1 = -L$ so that

$$T = \frac{K_{SE}F}{K_{LT} + K_{SE}} - \frac{K_{LT}K_{SE}\theta_1}{K_{LT} + K_{SE}}.$$

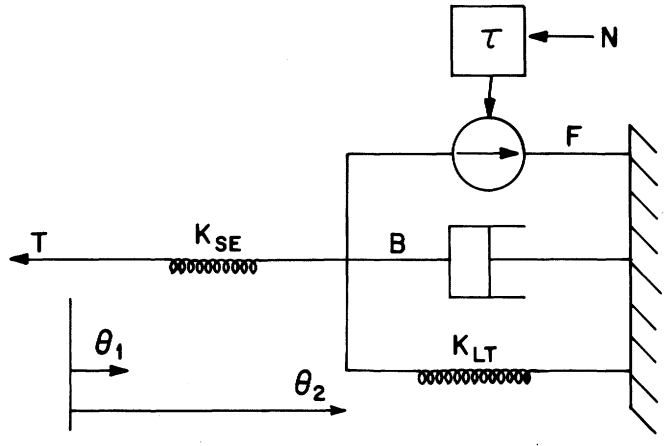

Fig. 4. Muscle model which includes a dashpot B that models the effects of the force-velocity relationship, and activation-deactivation time constants τ that model the conversion of motoneuronal firing N into active state tension F. Eye position is represented by θ_1.

We must now decrement this available force to account for the effects of the force-velocity relationship. The muscle force that is applied to the globe by the tendon becomes

$$T = \frac{K_{SE}F}{K_{LT}+K_{SE}} - \frac{K_{LT}K_{SE}\theta_1}{K_{LT}+K_{SE}} - B_{AG}\dot{\theta}_2. \tag{11}$$

The passive elasticity is the only muscle property not yet accounted for; it will be lumped in with the element K_p.

C. The Plant and System Equations

Our linear model can now be derived with reference to Fig. 5. Two muscles are pulling in opposite directions on the globe J. Their forces are

$$T_{AG} = K_{SE}(\theta_2 - \theta_1) \tag{12}$$

$$T_{ANT} = K_{SE}(\theta_1 - \theta_3). \tag{13}$$

From (11)

$$T_{AG} = \frac{K_{SE}F_{AG}}{K_{LT}+K_{SE}} - \frac{K_{LT}K_{SE}\theta_1}{K_{LT}+K_{SE}} - B_{AG}\dot{\theta}_2 \tag{14}$$

and

$$T_{ANT} = \frac{K_{SE}F_{ANT}}{K_{LT}+K_{SE}} + \frac{K_{LT}K_{SE}\theta_1}{K_{LT}+K_{SE}} + B_{ANT}\dot{\theta}_3. \tag{15}$$

The corresponding signs that are negative in (14) are positive in (15) because the antagonist dashpot adds to the resistive force of the antagonist active state tension and also, as the muscle gets longer, the length-tension diagram prescribes more muscle force which increases the resistive force.

Now (12) and (14) can be combined to yield

$$\frac{K_{SE}F_{AG}}{K_{LT}+K_{SE}} - \frac{K_{LT}K_{SE}\theta_1}{K_{LT}+K_{SE}} - B_{AG}\dot{\theta}_2 = K_{SE}(\theta_2 - \theta_1) \tag{16}$$

and (13) and (15) can be combined to yield

$$\frac{K_{SE}F_{ANT}}{K_{LT}+K_{SE}} + \frac{K_{LT}K_{SE}\theta_1}{K_{LT}+K_{SE}} + B_{ANT}\dot{\theta}_3 = K_{SE}(\theta_1 - \theta_3). \tag{17}$$

The two muscle forces acting on the globe [(12) and (13)] can be combined with the other forces acting on the globe to yield

$$K_{SE}(\theta_2 - \theta_1) - K_{SE}(\theta_1 - \theta_3) = K_p\theta_1 + B_p\dot{\theta}_1 + J\ddot{\theta}_1. \tag{18}$$

Equations (16)-(18) describe the movements of the model. However, the model is a sixth-order system, so it takes six differential equations to completely describe it. For these six state equations we will use the three positions, θ_1, θ_2, and θ_3, the eye velocity $\dot{\theta}_1$, and the two active state tensions, F_{AG} and F_{ANT}. We identify these state variables with the symbols x_1-x_6.

$x_1 = \theta_1$ = position of eye
$x_2 = \theta_2$ = position of agonist node, shown in Fig. 5
$x_3 = \theta_3$ = position of antagonist node, shown in Fig. 5
$x_4 = \dot{\theta}_1$ = eye velocity
$x_5 = F_{AG}$ = agonist active state tension
$x_6 = F_{ANT}$ = antagonist active state tension.

The inputs to the model are the neural control signals N_{AG} and N_{ANT}. These signals are transformed into the active state tensions by first-order activation and deactivation processes as shown in Fig. 6.

This is but one of many possible assignments for the state variables. This assignment happens to be intuitive and convenient. The three simultaneous equations [(16)-(18)] can be solved for each of the variables and three auxillary equations can be formed to yield the following six state equations:

$$\dot{x}_1 = x_4$$

$$\dot{x}_2 = \frac{K_{SE}^2}{(K_{LT}+K_{SE})B_{AG}}x_1 - \frac{K_{SE}}{B_{AG}}x_2 + \frac{K_{SE}}{(K_{LT}+K_{SE})B_{AG}}x_5$$

$$\dot{x}_3 = \frac{K_{SE}^2}{(K_{LT}+K_{SE})B_{ANT}}x_1 - \frac{K_{SE}}{B_{ANT}}x_3 - \frac{K_{SE}}{(K_{LT}+K_{SE})B_{ANT}}x_6$$

$$\dot{x}_4 = \frac{-2K_{SE}-K_p}{J}x_1 + \frac{K_{SE}}{J}x_2 + \frac{K_{SE}}{J}x_3 - \frac{B_p}{J}x_4$$

$$\dot{x}_5 = \frac{N_{AG}-x_5}{\tau_{AG}}$$

$$\dot{x}_6 = \frac{N_{ANT}-x_6}{\tau_{ANT}}.$$

The initial conditions are

$x_1(0) = x_4(0) = 0$
$x_2(0) = -x_3(0) = 1.1$ mm $= 5.6°$
$x_5(0) = x_6(0) = 0.2$ N $= 20.6$ gm tension.

These state equations completely describe the behavior of the model. It is sometimes more convenient to write these equations using matrix notation.

$$\dot{\boldsymbol{x}} = \boldsymbol{A}\boldsymbol{x} + \boldsymbol{B}\boldsymbol{u}.$$

In this equation $\dot{\boldsymbol{x}}$, $\boldsymbol{x}$, and $\boldsymbol{u}$ are vectors, $\boldsymbol{B}$ may be a vector or a matrix and $\boldsymbol{A}$ is a square matrix. Using this notation our six state equations become

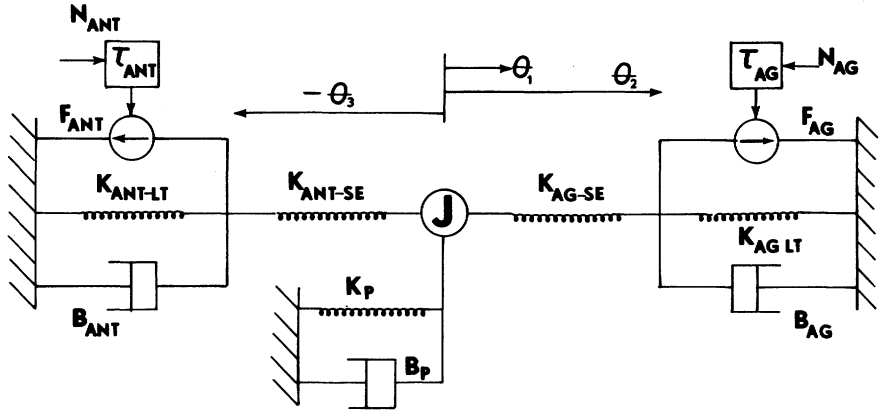

Fig. 5. The linear homeomorphic model. The globe and surrounding tissues were modeled by the effective inertia J, a viscous element B_p, and a passive elasticity K_p. (K_p also includes the passive elasticities of the muscles.) The agonist and antagonist muscles were, respectively, modeled by active state tension generators, F_{AG} and F_{ANT}, force-velocity relationship dashpots, B_{AG} and B_{ANT}, series elasticities, $K_{AG\text{-}SE}$ and $K_{ANT\text{-}SE}$, and length-tension elasticities, $K_{AG\text{-}LT}$ and $K_{ANT\text{-}LT}$. The active state tension generators convert oculomotoneuronal firing, N_{AG} and N_{ANT}, into force through first-order activation–deactivation processes, the τ's.

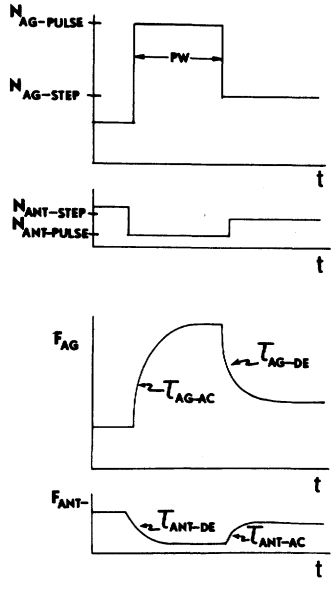

Fig. 6. The oculomotoneurons produce a pulse-step of firing N for saccadic eye movements. This firing pattern is converted into active state tension F by first-order activation and deactivation processes.

D. Parameter Values

The parameter values of Table I are given to complete the description of this model. Equations (4) and (7)-(10) appear directly. The neural signals, N_{AG} and N_{ANT}, are given units of force to avoid cumbersome conversion factors such as newton · second/motoneuronal spike. Forces are given in both newtons and gm tension because in the physiological literature muscle tensions are given in units of grams.

Length-tension and quick release experiments on the isolated globe [9]-[11] were used to determine the viscosity B_p and the elasticity K_p' of the globe orbit. The muscle passive elasticities were combined with K_p' to yield the element K_p. The inertial mass J was calculated based on a spherical radius of 11 mm and a density of 1 g/cc. Initial values for pulse-width, pulse height, and the four time constants were based upon the values used for 10° saccades in the old model. They are treated in greater detail in [23]. The parameter estimation program was then run and these six parameters were adjusted to yield the least mean squared error between the model and human responses. These values were then fixed for 10° sac-

$$\begin{bmatrix} \dot{x}_1 \\ \dot{x}_2 \\ \dot{x}_3 \\ \dot{x}_4 \\ \dot{x}_5 \\ \dot{x}_6 \end{bmatrix} = \begin{bmatrix} 0 & 0 & 0 & 1 & 0 & 0 \\ \dfrac{K_{SE}^2}{(K_{LT}+K_{SE})B_{AG}} & \dfrac{-K_{SE}}{B_{AG}} & 0 & 0 & \dfrac{K_{SE}}{(K_{LT}+K_{SE})B_{AG}} & 0 \\ \dfrac{K_{SE}^2}{(K_{LT}+K_{SE})B_{ANT}} & 0 & \dfrac{-K_{SE}}{B_{ANT}} & 0 & 0 & \dfrac{-K_{SE}}{(K_{LT}+K_{SE})B_{ANT}} \\ \dfrac{-2K_{SE}-K_p}{J} & \dfrac{K_{SE}}{J} & \dfrac{K_{SE}}{J} & \dfrac{-B_p}{J} & 0 & 0 \\ 0 & 0 & 0 & 0 & \dfrac{-1}{\tau_{AG}} & 0 \\ 0 & 0 & 0 & 0 & 0 & \dfrac{-1}{\tau_{ANT}} \end{bmatrix} \begin{bmatrix} x_1 \\ x_2 \\ x_3 \\ x_4 \\ x_5 \\ x_6 \end{bmatrix} + \begin{bmatrix} 0 \\ 0 \\ 0 \\ 0 \\ \dfrac{N_{AG}}{\tau_{AG}} \\ \dfrac{N_{ANT}}{\tau_{ANT}} \end{bmatrix}.$$

TABLE I
PARAMETER VALUES FOR THE LINEAR HOMEOMORPHIC MODEL

K_{SE} = 125 N/m = 2.5 gm tension/°
K_{LT} = 60 N/m = 1.2 gm/°
K_p = 25 N/m = 0.5 gm/°
B_p = 3.1 N · s/m = 0.06 gm · s/°
B_{AG} = 2.36 N · s/m = 0.046 gm · s/°
B_{ANT} = 1.12 N · s/m = 0.022 gm · s/°
J = 2.2 (10^{-3}) N · s^2/m = 4.3 (10^{-5}) gm · s^2/°
$N_{AG\text{-}PULSE}$ = PH = (0.54 + 0.11 $\Delta\theta$) N = (55 + 11 $\Delta\theta$) gm for $\Delta\theta \leqslant 11°$
= (1.57 + 0.02 $\Delta\theta$) N = (160 + 2 $\Delta\theta$) gm for $\Delta\theta > 11°$
$N_{ANT\text{-}PULSE}$ = 0.005 N = 0.5 gm
PW_{AG} = (10 + $\Delta\theta$) ms
PW_{ANT} = PW_{AG} + 6 ms
(antagonist pulse circumscribes agonist pulse by 3 ms on each end)
$N_{AG\text{-}STEP}$ = (0.2 + 0.02 θ) N = (20.6 + 2.35 θ) gm
$N_{ANT\text{-}STEP}$ = (0.2 − 0.007 θ) N = (20.6 − 0.74 θ) gm
$\tau_{AG\text{-}AC}$ = (11.7 − 0.2 $\Delta\theta$) ms
$\tau_{AG\text{-}DE}$ = 0.2 ms
$\tau_{ANT\text{-}AC}$ = 2.4 ms
$\tau_{ANT\text{-}DE}$ = 1.9 ms

cades. The parameter estimation routine was then run on a different size saccade adjusting pulsewidth, pulse height, and $\tau_{AG\text{-}AC}$ to minimize the error between model and human saccades. This procedure was repeated for saccades between 1° and 40°. Straight line approximations were then fit to these data points to yield the equations given below. The size of the intended saccade is $\Delta\theta$, and the intended final eye position is θ.

E. Simulations

This linear model yields good simulations for saccadic eye movements within ±20° of primary position (straight ahead). During ocular movements, the two eyes follow different trajectories [24]. The records of Fig. 7 show small differences between the two eyes. The left eye had a 9.7° saccade with a small amount of overshoot. The right eye had a 9.9° saccade with no overshoot. In order to quantify these differences the mean squared errors between the model and human saccades were computed for 120 ms simulations. The mean squared error between the 9.7° model saccade and the human saccade of the left eye in Fig. 7 was 51 X 10^{-6} deg^2. The mean squared error between the 9.9° model saccade and the human saccade of the right eye in Fig. 7 was 21 X 10^{-6} deg^2. The mean squared error between the saccades of the two eyes was 107 X 10^{-6} deg^2. The parameter estimation program has shown that the differences shown in Fig. 7 could be produced with small variations in pulse height and pulsewidth. Increasing the pulse height 6 percent above its nominal value and simultaneously increasing the pulsewidth 2 percent above its nominal value reduced the mean squared error between the model and the left eye from 51 to 41 X 10^{-6} deg^2. Increasing the pulse height 2 percent above its nominal value was sufficient to reduce the mean squared error between the model and the right eye from 21 to 18 X 10^{-6} deg^2. If, in addition to pulse height and pulsewidth, the four time constants and the agonist and antagonist dashpot values were also varied, then the mean squared error for the left eye could be reduced to 35 X 10^{-6} deg^2, and the error for the right eye could be reduced to 16 X 10^{-6} deg^2.

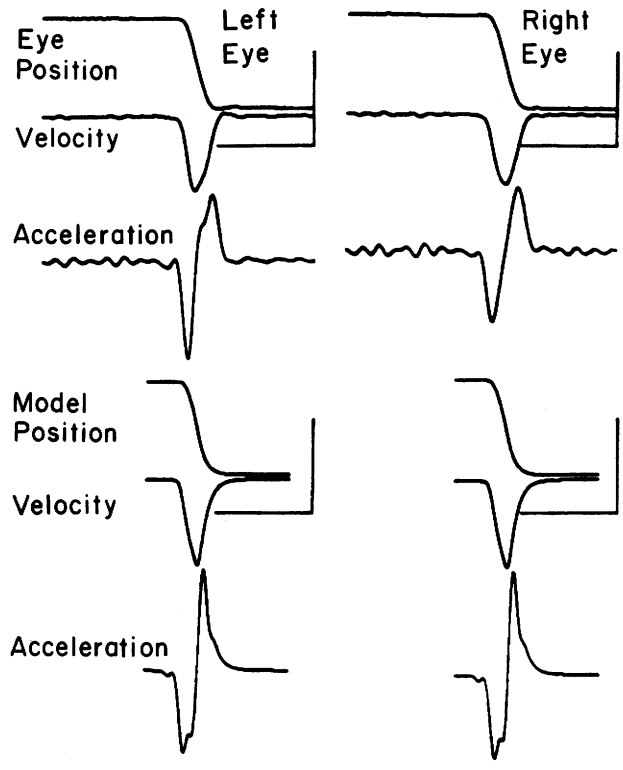

Fig. 7. Human (top) and model (bottom) 10° saccadic eye movements with small differences between the simultaneous saccades of the right and left eyes. The left column (the left eye) and the right column (the right eye) show from top to bottom eye position, eye velocity, and eye acceleration all as functions of time. Eye position, velocity, and acceleration bandwidths were, respectively, 300, 80, and 60 Hz for the model and the human data. Small changes in pulse height and pulsewidth were sufficient to match the right-eye left-eye differences of the human records. Upward deflections represent rightward movements. The calibration bar represents 10°, 500°/s, 30 000°/s^2, and 100 ms.

Model glissades that quantitatively match human glissades of normals can only be produced by pulsewidth variations. In order to minimize the mean squared error between the human eye movement with the glissadic undershoot, illustrated in the right column of Fig. 8, the pulsewidth had to be decreased by a large amount. When the parameter estimation routine was allowed to vary the pulsewidth and the pulse height (the only two physiological parameters that are likely to change between saccades) the best fit was obtained by decreasing the pulsewidth 16 percent below its nominal value, while decreasing the pulse height 2.5 percent below its nominal value. This saccadic eye movement moved the eye 19.7°: the dynamic saccade moved it 17.7°, and the glissade moved it another 2°. The nominal values for a 19.7° saccade are 29.7 ms for the pulsewidth and 199 gm for the pulse height. These values produced a mean squared error of 3100 X 10^{-6} deg^2. The values that gave the best simulation were 25 ms for the pulsewidth and 194 gm for the pulse height. The mean squared error for a 120 ms simulation was 273 X 10^{-6} deg^2. When our estimation program was allowed to vary pulsewidth, pulse height, and the four time constants, the fit was not improved. Similarly, the glissadic overshoot shown in the left column of

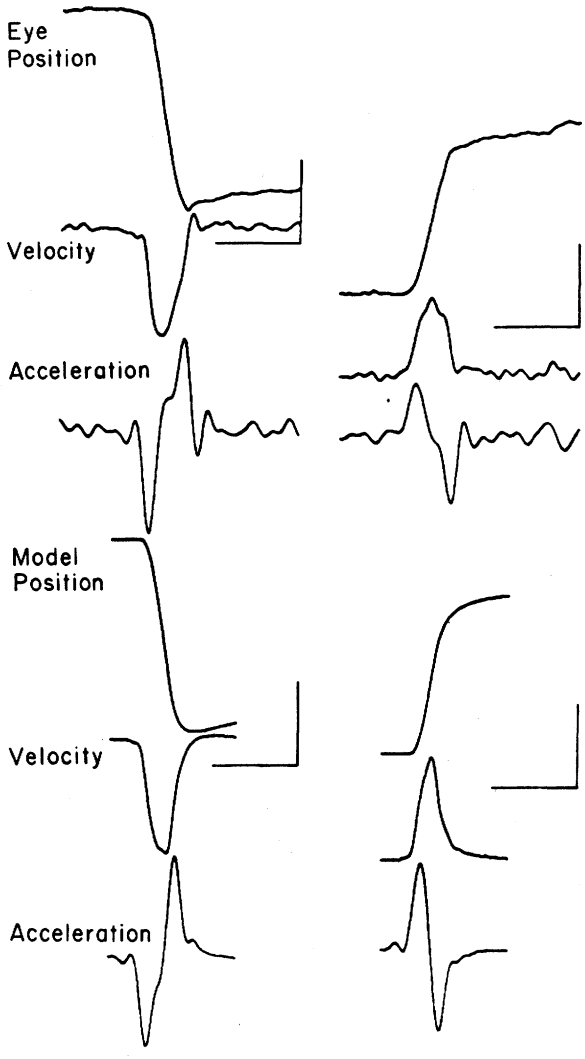

Fig. 8. Human (top) and model (bottom) 20° saccadic eye movements with large differences between two consecutive saccades of the right eye. The left column is a leftward movement and the right column is the subsequent rightward movement. Glissades such as these are caused by pulsewidth errors. This pattern is similar to those of patients with multiple sclerosis. To simulate such movements (minimizing the mean squared error between the model and human outputs) the pulsewidth in the model had to be decreased 16 percent below its nominal value to produce the glissadic undershoot in the right column. The model pulsewidth had to be increased 12 percent above its nominal value to produce the overshoot in the left column. In both cases the pulse height had to be held within 3 percent of its nominal value. Bandwidths were 125, 60, and 45 Hz, respectively, for the eye position, eye velocity, and eye acceleration records. The calibration bar represents 10°, 500°/s, 30 000°/s^2, and 100 ms.

Fig. 8 could be fit best by making large pulsewidth changes. The best fit was obtained with a 12 percent increase in pulsewidth and a 1 percent decrease in pulse height. This saccadic eye movement moved the eye 20.8° from start to finish: the dynamic saccade moved the eye 24° and the glissade brought it back 3.2°. The nominal values for a 20.8° saccade are 30.8 ms for the pulsewidth and 202 gm for the pulse height. These values produced a mean squared error of 1500×10^{-6} deg^2. The values that gave the best simulation were 34.6 ms and 200 gm. The mean squared error was 136×10^{-6} deg^2. Changing all eight parameters simultaneously decreased the mean squared error by 3 percent.

This confirms the suggestion of Bahill *et al.* [25] that glissadic *overshoot* in normals is caused by pulsewidth errors. Furthermore, it also shows that glissadic *undershoots* are caused by pulsewidth errors and not pulse height errors. Using the parameter estimation routine to draw these conclusions was simpler than the previous method [25]. Furthermore, it also ruled out a combination of pulsewidth and pulse height errors as the cause of glissades. These results imply that central nervous system mechanisms can control the height of a motoneuronal burst quite accurately, but it is more difficult to control the duration of a motoneuronal burst.

F. Goodness of Fit

To evaluate the goodness of fit of existing eye movement models the differences between the outputs of several models and some typical human saccadic eye movements were computed. 10° saccades of a normal unfatigued human were recorded and the first 16 of these were used to test the goodness of fit of the models. Each model was run for 60 ms. The resulting record was then compared point by point to the human saccadic eye movement, and the mean squared error was calculated. This process was repeated 50 times as the model was shifted forward and backward in time. The shift with the minimum mean squared error was chosen as the best possible fit for that model. This process was then repeated for each of the 16 saccades and the mean and standard deviation of the mean squared errors were computed. The results are shown in Table II. The linear homeomorphic model had the least mean squared error.

For the linear homeomorphic model the simulations match the human eye movements almost as well as the two eyes match each other. Biological variations produce larger differences in saccadic trajectories than those caused by small parameter adjustments. This implies that the model parameters have been selected optimally; further modifications are not likely to be useful. This is an excellent general model for eye movements. By using the parameter estimation routine the mean squared error can be minimized for any specific saccadic eye movement.

III. Discussion

The control of eye movements is easier to study than the control of other neuromuscular systems as explained in the introduction and also because of the fact that the eyeballs do not exhibit six degrees of freedom. Translational movements are extremely small, so only the three degrees of rotational freedom remain. However, the eyeballs do not ordinarily demonstrate three degrees of rotational freedom. In between movements only two parameters specify the position of the eye; there is one and only one torsional position for any given direction of line of sight. This principle is called Listing's Law. For any direction of gaze the neural signals for all of the extraocular muscles are fixed. By contrast, if you move your finger from the left side of this page to the right side you may do so by varying wrist, elbow, and shoulder joints. Each time the same point is reached there may be an entirely different set of joint angles and muscle forces.

TABLE II
MEAN AND STANDARD DEVIATION OF THE MEAN SQUARED ERRORS ($\times 10^{-6}$deg^2) BETWEEN 60 ms SIMULATIONS OF VARIOUS MODELS AND 16 HUMAN 10° SACCADIC EYE MOVEMENTS

Model Description	Reference	Error in Matching Human Saccades
zero-order, $\frac{\theta_{eye}}{input} = 1$	[26]	3507 ± 198
second-order, linear, overdamped $\tau_1 = 150$ ms, $\tau_2 = 12$ ms, with integrator and pulse input	[27]	2759 ± 822
sixth-order, linear model without length-tension element	[22]	275 ± 324
second-order, linear, underdamped $\omega_n = 120$ rad/s, $\zeta = 0.7$, step input	[2]	250 ± 150
sixth-order, nonlinear model without length-tension diagram	[7]	136 ± 60
sixth-order, nonlinear model with length-tension element	unpublished data	57 ± 31
sixth-order, linear model with length-tension element	Fig. 5 and Table I	52 ± 24
left eye trying to match the right eye	this report	45 ± 20

The mean squared error between human and model saccades was seldom zero. The model is sixth-order, linear, and deterministic: the physiological system is not sixth-order, is not linear, and is corrupted by stochastic noise. Therefore, it would not be expected that the mean squared error could be reduced to zero for any particular saccade. Furthermore, certain saccadic eye movements are produced by controller signals that are more complex than those shown in Fig. 6. For example, the saccadic eye movement of the left eye shown in Fig. 7 has a small amount of dynamic overshoot. A better simulation requires controller signals for two saccades: a 9.7° primary saccade and a 0.2° return saccade [6]. Almost all of the error in matching this particular saccade occurred at the end of the movement when the human saccade was exhibiting this dynamic overshoot.

There are two major reasons why the mean squared errors between the model and human saccadic eye movements of Fig. 8 are larger than those of Fig. 7. First, the records of Fig. 8 are more noisy. This noise is primarily due to movements of the lid and orbital tissues. Sometimes it can be minimized by a longer and more careful adjustment of the photocells. It is stochastic so a noise free model will not be able to match the records as well. Second, in the left column of Fig. 8 the eye starts drifting toward the new target position 10–20 ms before the saccade starts; the model will not produce such presaccadic drifts.

The pulse height values used in the model are larger than the muscle forces of Fig. 1. One reason for this is that the data of Fig. 1 are for static fixations; the muscle forces during saccades are larger. Furthermore, the pulse height is not equal to the muscle force; there is a large amount of shaping done by the various elements of the model. For example, for a 10° saccade $N_{AG\text{-}pulse}$ is 165 gm. This 165 gm neural pulse is reduced to a 146 gm active state tension, which is further reduced by the passive elasticity, the length-tension elasticity, and the agonist dashpot to produce a total peak muscle force of 93 gm. This value is larger than the 30–70 gm muscle forces reported during human saccades [9], [10]. The agonist deactivation time constant is also smaller than was implied in these studies. The fact that a larger force and a smaller time constant were needed to minimize the error between the human and model saccades suggests areas for future research.

The model was simulated by using a multistep Adams-Moulton predictor-corrector algorithm to numerically solve the differential equations with a Runge-Kutta routine used for the starting values. All programs were written in *C*, the language of Bell Laboratory's Unix operating system.

There are many reasons why we linearized the model. First, a sensitivity analysis [7] showed that the force-velocity dashpot parameters (the cause of the nonlinearities) had large effects on the model response, yet the data for these parameters were not robust. Therefore, the treatment of the dashpots had to be revised and one method for doing this was linearization. Second, data for the force-velocity relationship came from turtle, frog, cat, and rat, but not from man. There was a great deal of variability depending upon the species, the type of muscle, the laboratory, and the experimental conditions. Given the noise and uncertainty in the data, a linear approximation to the data was as good as a nonlinear approximation. Third, the linear model is simpler and should, therefore, have greater portability. Fourth, when a model is linear the model can be validated using classical engineering tools. For example, existing computer programs [28] can be used to assess stability and compute root locus plots. Fifth, linear systems obey the principle of superposition which makes most analyses easier. For example, in the sensitivity analysis [7] of the old nonlinear model one parameter at a time was varied. Yet it is possible that the interaction of two parameters could have had a greater effect on the model than merely the sum of their two individual effects. Thus, this whole validation technique could reasonably be questioned. With the linear model it was sufficient to vary only one parameter at a time in the sensitivity analysis. Sixth, parameter estimation programs are more likely to find a unique optimal solution for a linear model. In summary, the linear model matches the physiological data and the human output response better than the nonlinear model. The linear model is simpler, and provides the opportunity to apply the tools and tests of control theory in order to validate the model.

REFERENCES

[1] R. Descartes, *Treatise of Man*, originally published by C. Angot, Paris, France, 1664; republished with translation and commentary by T. S. Hall, Cambridge, MA: Harvard Univ. Press, 1972, pp. 22–30.
[2] G. Westheimer, "Mechanism of saccadic eye movements," *Amer. Med. Assoc. Arch. Ophthamol.*, vol. 52, pp. 710–724, 1954.
[3] D. A. Robinson, "The mechanics of human saccadic eye movement," *J. Physiol.*, vol. 174, pp. 245–264, 1964.
[4] G. Cook and L. Stark, "The human eye movement mechanism: Experiments, modeling and model testing," *Arch. Opthalmol.*, vol. 79, pp. 428–436, 1968.
[5] M. R. Clark and L. Stark, "Control of human eye movements," *Math. Biosci.*, vol. 20, pp. 191–265, 1974.
[6] A. T. Bahill, M. R. Clark, and L. Stark, "Dynamic overshoot in saccadic eye movements is caused by neurological control signal reversals," *Exper. Neurol.*, vol. 48, pp. 95–122, 1975.
[7] F. K. Hsu, A. T. Bahill, and L. Stark, "Parametric sensitivity of a

homeomorphic model for saccadic and vergence eye movements," *Comput. Prog. Biomed.*, vol. 6, pp. 108–116, 1976.
[8] A. T. Bahill, F. K. Hsu, and L. Stark, "Development, sensitivity analysis and predictions of a reciprocal innervation model for saccadic and vergence eye movements," in *Modeling and Simulation, Proc. 7th Annu. Pittsburgh Conf.*, W. Vogt, and M. Mickle, Eds. Pittsburgh, PA: Instrument Society of America, 1976, pp. 1245–1250.
[9] D. A. Robinson, D. M. O'Meara, A. B. Scott, and C. C. Collins, "Mechanical components of human eye movements," *J. Appl. Physiol.*, vol. 26, pp. 548–553, 1969.
[10] C. C. Collins, D. O'Meara, and A. B. Scott, "Muscle tension during unrestrained human eye movements," *J. Physiol.*, vol. 245, pp. 351–369, 1975.
[11] C. C. Collins, "The human oculomotor control system," in *Basic Mechanisms of Ocular Motility and Their Clinical Implications*, G. Lennerstrand and P. Bach-y-Rita, Eds. New York: Pergamon, 1975, pp. 145–180.
[12] A. V. Hill, "The heat of shortening and dynamic constraints of muscle," *Proc. Royal Society, London, (Ser. B)*, vol. 126, pp. 136–195, 1938.
[13] M. R. Clark, E. I. Jury, V. V. Krishnan, and L. Stark, "Computer simulation of biological models using the inners approach," *Comput. Prog. Biomed.*, vol. 5, pp. 263–282, 1975.
[14] J. R. Latimer, B. T. Troost, and A. T. Bahill, "Linearization and sensitivity analysis of model for human eye movements," in *Modeling and Simulation, Proc. 9th Annu. Pittsburgh Conf.*, W. Vogt and M. Mickle, Eds. Pittsburgh, PA: Instrument Society of America, 1978, pp. 365–371.
[15] L. Stark, *Neurological Control Systems, Studies in Bioengineering*. New York: Plenum, 1968, pp. 308–312.
[16] A. M. Gordon, A. F. Huxley, and F. J. Julian, "The variation in isometric tension with sarcomere length in vertebrate muscle fibers," *J. Physiol.*, vol. 184, pp. 170–192, 1966.
[17] G. C. Joyce and P. M. H. Rack, "Isotonic lengthening and shortening movements of cat soleus muscle," *J. Physiol.*, vol. 204, pp. 475–491, 1969.
[18] G. G. Joyce, P. M. H. Rack, and D. R. Westbury, "The mechanical properties of cat soleus muscle during controlled lengthening and shortening movements," *J. Physiol.*, vol. 204, pp. 461–474, 1969.
[19] F. J. Julian, "The effect of calcium on the force-velocity relation of briefly glycerinated frog muscle fibers," *J. Physiol.*, vol. 218, pp. 117–145, 1971.
[20] F. J. Julian and M. R. Sollins, "Regulation of force and speed of shortening in muscle contraction," in *Cold Springs Harbor Symp. Quantitative Biol.*, vol. 37, 1973, pp. 635–646.
[21] L. D. Partridge, "Muscle properties: A problem for the motor physiologist," in *Posture and Movement: Prospective for Integrating Sensory and Motor Research on the Mammalian Nervous System*, R. E. Talbott and D. R. Humphrey, Eds. New York: Raven, 1979, pp. 189–229.
[22] J. R. Latimer and A. T. Bahill, "Parameter estimation by function minimization using a modified steepest descent method," in *Modeling and Simulation, Proc. 10th Annu. Pittsburgh Conf.*, W. Vogt and M. Mickle, Eds. Pittsburgh, PA: Instrument Society of America, 1979, pp. 683–690.
[23] A. T. Bahill, "Development, validation and sensitivity analyses of human eye movement models," *CRC Crit. Rev. Bioeng.*, vol. 4, issue 4, 1980, in press.
[24] A. T. Bahill, K. J. Ciuffreda, R. V. Kenyon, and L. Stark, "Dynamic and static violations of Hering's law of equal innervation," *Amer. J. Optom. Physiol. Optics*, vol. 53, pp. 786–796, 1976.
[25] A. T. Bahill, F. K. Hsu, and L. Stark, "Glissadic overshoots are due to pulse width errors," *Arch. Neurol.*, vol. 35, pp. 138–142, 1978.
[26] J. B. Selhorst, L. Stark, A. L. Ochs, and W. F. Hoyt, "Disorders in cerebellar oculomotor control," *Brain*, vol. 99, pp. 497–522, 1976.
[27] D. A. Robinson, "Models of the saccadic eye movement control system," *Kybernetik*, vol. 14, pp. 71–83, 1973.
[28] J. L. Melsa and S. K. Jones, *Computer Programs for Computational Assistance in the Study of Linear Control Theory*. New York: McGraw-Hill, 1970.

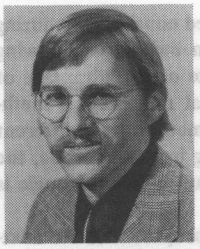

A. Terry Bahill (S'66–M'68) was born in Washington, PA, on January 31, 1946. He received the B.S.E.E. degree in electrical engineering from the University of Arizona, Tucson, in 1967, the M.S.E.E. degree in electrical engineering from San Jose State University, San Jose, CA, in 1970, and the Ph.D. in electrical engineering and computer science from the University of California, Berkeley, in 1975.

He served as a Lieutenant in the U.S. Navy teaching mathematics and electrical engineering for 4 years to the students of the Navy Nuclear Power School, Mare Island, CA. He has been at Carnegie-Mellon University, Pittsburgh, PA, since 1976. His research interests include control theory, bioinstrumentation, modeling physiological systems, model validation, and real-time computer systems. He has recently written a textbook on bioengineering.

Dr. Bahill is a member of the IEEE Engineering in Medicine and Biology and Systems, Man, and Cybernetics Societies. He is on the Administrative Committee of the latter. He is a member of Tau Beta Pi, Sigma Xi, Psi Chi, and is a Registered Professional Engineer.

Jose R. Latimer was born on February 11, 1955. He received the B.E. degree in electrical engineering from Villanova University, Villanova, PA, in 1977, and the M.S. degree in electrical engineering–bioengineering from Carnegie-Mellon University, Pittsburgh, PA, in 1979.

He is now with the Applied Physics Laboratory, The Johns Hopkins University, Baltimore, MD. His current interests are in system identification, estimation, modeling, and applied systems and control theory.

Mr. Latimer is a member of Tau Beta Pi, Phi Kappa Phi, and Sigma Xi.

B. Todd Troost was born in Mankato, MN, on July 5, 1937. He received the B.S. degree in biophysics from Yale University, New Haven, CT, in 1959, and the M.D. degree in medicine from Harvard University, Boston, MA, in 1963.

He completed specialty training in neurology at the University of Colorado Medical Center, Denver, and pursued neuro-ophthalmology at the University of California, San Francisco, and at the University of Miami School of Medicine, Miami, FL. Currently, he is with the Department of Neurology, Case Western Reserve University, Cleveland, OH. His research interests include ocular motor neurophysiology, control theory, and computer applications in medicine.

Dr. Troost is Board Certified in Neurology, a member of the American Neurological Association, and a Fellow of the American Academy of Neurology.